

# Radio emission from dark matter annihilation in the Large Magellanic Cloud

Beatriz B. Siffert,<sup>1\*</sup> Angelo Limone,<sup>1</sup> Enrico Borriello,<sup>1,2</sup> Giuseppe Longo<sup>1,3,4</sup>  
and Gennaro Miele<sup>1,2</sup>

<sup>1</sup>*Dipartimento di Scienze Fisiche, Università di Napoli Federico II, Via Cinthia, 9, I-80126 Naples, Italy*

<sup>2</sup>*INFN - Sezione di Napoli, Via Cinthia, 9, I-80126 Naples, Italy*

<sup>3</sup>*INAF-OACN, Via Moirariello, 16, I-80128 Naples, Italy*

<sup>4</sup>*Department of Astronomy, California Institute of Technology, 1200 East California Blvd, Pasadena, CA 91125, USA*

Accepted 2010 August 29. Received 2010 August 27; in original form 2010 July 1

## ABSTRACT

The Large Magellanic Cloud (LMC), at only 50 kpc away from us and known to be dark matter dominated, is clearly an interesting place where to search for dark matter annihilation signals. In this paper, we estimate the synchrotron emission due to weakly interacting massive particle (WIMP) annihilation in the halo of the LMC at two radio frequencies, 1.4 and 4.8 GHz, and compare it to the observed emission, in order to impose constraints in the WIMP mass versus annihilation cross-section plane. We use available Faraday rotation data from background sources to estimate the magnitude of the magnetic field in different regions of the LMC's disc, where we calculate the radio signal due to dark matter annihilation. We account for the  $e^+e^-$  energy losses due to synchrotron, inverse Compton scattering and bremsstrahlung, using the observed hydrogen and dust temperature distribution on the LMC to estimate their efficiency. The extensive use of observations, allied with conservative choices adopted in all the steps of the calculation, allows us to obtain very realistic constraints.

**Key words:** magnetic fields – galaxies: individual: Large Magellanic Cloud – dark matter – radio continuum: galaxies.

## 1 INTRODUCTION

Evidence for the existence of dark matter (DM) has been observed in various astrophysical systems, ranging from satellite dwarf galaxies to massive galaxy clusters and cosmology. Possible cold dark matter (CDM) candidates arise from theoretical models conceived to extend the Standard Model of elementary particles and weakly interacting massive particles (WIMPs) are the current main paradigm (see Feng 2010 for a recent review on DM candidates).

The fact that a direct observation of DM particles has not yet been possible justifies all the efforts devoted to their indirect detection, that is, the observation of anomalous components in the cosmic rays' spectrum that can be attributed to DM annihilation. See Crocker et al. (2010), Abdo et al. (2010), Bergstrom, Fairbairn & Pieri (2006), Barger et al. (2002), Colafrancesco, Profumo & Ullio (2006) and Colafrancesco, Profumo & Ullio (2007) for examples of such searches in the  $\gamma$ -ray, X-ray and neutrino spectra, and Aloisio, Blasi & Olinto (2004), Zhang & Sigl (2008), Baltz & Wai (2004), Blasi, Olinto & Tyler (2003) and Hooper (2008) for the radio band.

In fact, DM self-annihilation is expected to produce several Standard Model particles, among which electrons and positrons that,

by interacting with the galactic magnetic field, emit synchrotron radiation in the radio band. We can estimate the intensity of the emission coming from a given direction in the sky by adopting models or using measurements to describe the following quantities: the DM density profile, which can be modelled by using the results of halo formation numerical simulations; the magnetic field, estimated through techniques, such as the analysis of polarization of radio and optical emission and rotation measures (RMs); and the interstellar radiation field (ISRF) and hydrogen distribution, which are needed to account for the electron/positron energy losses. The comparison of this emission with the observed radio emission then allows to impose constraints on the values of the DM particle's mass,  $m_\chi$ , and its thermally averaged annihilation cross-section,  $\langle\sigma_A v\rangle$ .

In order for this method to provide reliable constraints, the values of all the involved parameters need to be known very well, which often does not happen. Furthermore, ideally, the comparison between the theoretical result and the observed emission should be made after all the known astrophysical foregrounds have been subtracted from the observations. In practice, however, such subtraction is subject to several uncertainties, since often we cannot accurately model all the components contributing to the foreground.

In addition, the method presents an intrinsic shortcoming: we can only calculate the contributions from DM annihilation integrated

\*E-mail: siffert@na.infn.it; beatriz@ifoufrj.br

along the line of sight, so all the DM signal may be ‘averaged’ away by low emitting regions that happen to fall along the same direction in the sky.

In this paper, we present constraints obtained by applying this method to the Large Magellanic Cloud (LMC) and comparing the results with radio observations at 1.4 and 4.8 GHz. Unless otherwise stated, we will follow the formalism described in Borriello, Cuoco & Miele (2009) in our calculations. We analyse two possible WIMP annihilation channels, a hadronic and a leptonic one, the latter having been recently proposed as a possible cause of the anomalous cosmic-ray electron/positron spectrum measured by PAMELA (Adriani et al. 2009) and Fermi–LAT (Abdo et al. 2009).

By extensive use of available observations of the LMC in different frequencies, we are able to obtain realistic information to describe all the inputs necessary to estimate the DM annihilation signal. In this way, we escape from the ‘too-many-hypotheses’ problem that has recurrently appeared in the existing literature on the subject. When we do have to make a hypothesis, we follow the most conservative path, making sure that our choice will not overestimate the signal.

The LMC, at a distance of only  $\sim 50$  kpc from us (Alves 2004), is probably one of the best-studied galaxies in almost all frequency bands. Rotation curve data imply that the LMC’s total mass inside a 9 kpc radius is  $\sim 1.3 \times 10^{10} M_{\odot}$ , while the sum of the stellar and neutral gas masses is estimated to be  $\sim 3.2 \times 10^9 M_{\odot}$  (van der Marel, Kallivayalil & Besla 2009). Therefore, the LMC must be DM dominated.

The fact that the LMC is nearly face-on (its disc forms an angle of  $\sim 35^\circ$  with the plane of the sky, van der Marel & Cioni 2001) minimizes the line of sight integration problem mentioned above, since, in this case, the integration spans only over the thickness of the galaxy. A nearly face-on view also allows us to clearly distinguish between high emitting and low emitting regions within the disc, that is, between regions where different astrophysical processes are taking place and where different astrophysical foregrounds exist.

In Borriello et al. (2010), some of the authors of this paper looked for DM annihilation from low radio emitting regions (called ‘radio cavities’) within the nearly face-on Local Group member Messier 33 (inclination  $56^\circ$ ). Following this reference, a good candidate radio cavity should present low radio emission relative to the rest of the disc and should not be very far from the centre of the galaxy. While the first criterion guarantees that the astrophysical foreground in that region is relatively small, the second one is required so that the DM density is non-negligible and that the possibility of a high magnetic field is not ruled out. Although this study produced constraints comparable to those obtained for the Milky Way (see e.g. Borriello et al. 2009), the lack of knowledge of the values of the astrophysical environment governing the diffusion of the electrons and positrons, in particular the magnetic field, introduces several uncertainties on the results.

In the present analysis, in contrast, we use recent accurate RMs from point sources behind the LMC obtained in Gaensler et al. (2005), through which we can directly estimate the magnitude of the magnetic field in several regions for the disc of the LMC. We focus our analysis on 23 regions on the LMC’s disc with galactocentric distances  $\lesssim 8$  kpc for which an RM has been measured. Although these regions are not chosen to be radio cavities, the fact that a background radio source has been seen there guarantees that they present low radio emission in comparison to other parts of the galaxy (intensity at 1.4 and 4.8 GHz  $\lesssim 2$  mJy beam $^{-1}$ ). For each of these regions, we calculate the expected DM emission at 1.4 and 4.8 GHz and compare the results with the observed values without

performing any foreground subtraction (which is a conservative choice, since removing part of the observed emission would always strengthen the constraints).

Previous searches for DM annihilation signals from the LMC have analysed both the  $\gamma$ -ray (Gondolo 1994; Tasitsiomi, Gaskins & Olinto 2004) and radio (Tasitsiomi et al. 2004) bands. In particular, in the latter, the flux density in several radio frequencies due to annihilation into the hadronic channel integrated over the entire galaxy is calculated. However, unlike what is done here, in Tasitsiomi et al. (2004) a simple constant magnetic field inside the entire volume of the galaxy is assumed. Furthermore, electron/positron energy losses due to inverse Compton scattering (ICS) and bremsstrahlung are neglected in Tasitsiomi et al. (2004), although, as we show in section 4, these processes can be very important in several regions of the LMC. When appropriate, we will comment on the effect of these assumptions and compare our results with theirs.

This paper is organized as follows. In Section 2, we present the radio data used in our analysis and the 23 regions studied. Section 3 is dedicated to the distribution of DM in the halo of the LMC and presents the results of fits to different DM profiles. In Section 4, we discuss the energy-loss processes relevant to our calculations. In section 5, we present our results and discuss them and compare with previous ones in Section 6.

## 2 RADIO DATA AND SELECTION OF REGIONS

We used radio observations of the LMC at two different frequencies, 1.4 and 4.8 GHz. At 1.4 GHz, we used the mosaic image obtained with the Australia Telescope Compact Array (ATCA) and the Parkes Telescope (Hughes et al. 2007), shown in the left-hand panel of Fig. 1. The beam width (HPBW) for this image is 40 arcsec, which corresponds to  $\sim 10$  pc at the LMC’s position, and its sensitivity is estimated to be between 0.25 and 0.35 mJy beam $^{-1}$ . At 4.8 GHz, we used the observations made with the ATCA described in Dickel et al. (2005) and shown in the right-hand panel of Fig. 1. The HPBW is 33 arcsec and the estimated sensitivity is 0.28 mJy beam $^{-1}$ .

We estimated the radio emission due to DM annihilation at these two frequencies coming from 23 circular regions with radius 180 arcsec within the LMC’s disc. The selection of regions was made according to the results presented in Gaensler et al. (2005), where the Faraday rotation for 291 polarized sources behind the LMC was measured, 100 of which happen to lie directly behind the LMC. After subtracting the effects due to the foreground Faraday rotation in the Milky Way, a map of RMs is obtained (fig. 1 in Gaensler et al. 2005), where circles of various sizes represent the magnitude of the RM at each position. We chose the positions of 23 circles to apply our method, selecting them according to their diameter, which is proportional to the RM at that position (large RM implies large magnetic field and therefore large synchrotron emission), and distance from the centre of the LMC (as we move away from the centre the density of DM decreases). In our calculations, we used the LMC’s kinematic centre, with coordinates RA =  $05^{\text{h}}17^{\text{m}}36^{\text{s}}$  and Dec. =  $-69^\circ 02'$  (Kim et al. 1998).

Since the data published in Gaensler et al. (2005) are not yet of public domain, we had to obtain the positions and the RM of each of the 23 regions directly from the map in their fig. 1, using the fact that the maximum RM measured is  $+247 \pm 13$  rad m $^{-2}$ . To help us determine the coordinates of each region, we used the list of sources published in Marx, Dickey & Mebold (1997), which contains 113 compact radio sources detected with the ATCA at 1.4 GHz in and behind the LMC, in a region comprehended between  $05^{\text{h}}17^{\text{m}} \lesssim \text{RA} \lesssim 05^{\text{h}}51^{\text{m}}$  and  $-71^\circ \lesssim \text{Dec.} \lesssim -67^\circ$ . It is estimated

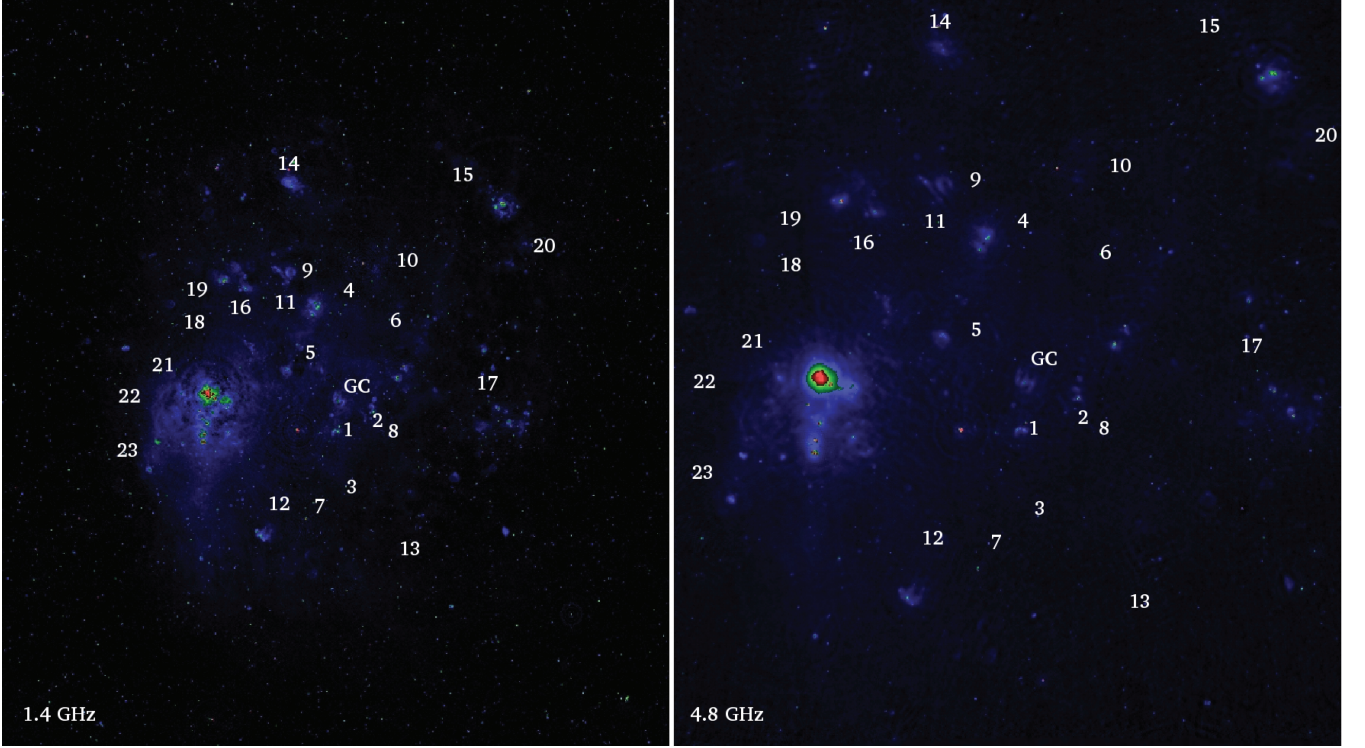


**Figure 1.** Radio maps in a logarithmic scale of the LMC at 1.4 GHz (Hughes et al. 2007) and 4.8 GHz (Dickel et al. 2005). The numbers indicate the positions of the 23 selected regions where the Faraday rotation of background sources is measured. The label ‘GC’ indicates the assumed LMC’s kinematic centre.

that among these 113 sources, 15 are in the LMC, so most of them are background objects.

Once RMs have been estimated for each region, the corresponding magnetic field was obtained using the definition

$$\text{RM} = k \int n_e B_{\text{reg}\parallel} ds, \quad (1)$$

where  $k = 0.81 \text{ rad m}^{-2} \text{ pc}^{-1} \text{ cm}^3 \mu\text{G}^{-1}$ ,  $n_e$  is the electron number density,  $B_{\text{reg}\parallel}$  is the regular component of the magnetic field parallel to line of sight and  $s$  is the distance along the line of sight.

Assuming that the regular component of the magnetic field,  $B_{\text{reg}}$ , lies solely on the plane of the disc, we conclude that  $B_{\text{reg}\parallel}$  is produced by the galaxy’s inclination. The mean value of  $B_{\text{reg}}$ , weighted according to the electron density  $n_e$  along the line of sight, is then given by

$$B_{\text{reg}} = \frac{\text{RM}}{k \mathcal{DM} \sin i}, \quad (2)$$

where  $\mathcal{DM}$  is the dispersion measure, defined as  $\int n_e ds$  and  $i \sim 35^\circ$  is the LMC’s disc inclination. In our calculations, we used the mean total dispersion measure calculated from five radio pulsars in the LMC obtained in Crawford et al. (2001),  $\mathcal{DM} = 100 \text{ cm}^{-3} \text{ pc}$ , following what was done in Gaensler et al. (2005).

In Gaensler et al. (2005), the random component of the LMC’s magnetic field,  $B_{\text{ran}}$ , was estimated to be  $\sim 3.6 B_{\text{reg}}$ , so that  $B_{\text{tot}} = \sqrt{B_{\text{reg}}^2 + B_{\text{ran}}^2} \simeq 3.7 B_{\text{reg}}$ . As mentioned in Gaensler et al. (2005), in regions where the magnetic field and  $n_e$  are correlated, the above calculation overestimates  $B_{\text{reg}}$  by a factor of 2 and underestimates  $B_{\text{ran}}$  by the same factor.

The 23 selected regions are shown in Fig. 1, superimposed to the radio maps. They are numbered from the smallest to the largest

galactocentric distance. In Table 1, we list for each region its equatorial coordinates, corresponding background source name as in Marx et al. (1997), if any, distance to the centre of the LMC along the plane of the disc, assuming a distance to the LMC of 50 kpc, regular and total magnetic fields estimated from the RM, ISRF on the disc (see Section 4), the atomic hydrogen number density (see Section 4) and intensity measured at 1.4 and 4.8 GHz. The values of intensity at 4.8 GHz marked with an asterisk were lower than the corresponding sensitivity and were set to the sensitivity value,  $0.28 \text{ mJy beam}^{-1}$ .

To model the behaviour of the magnetic field along the  $z$ -axis (perpendicular to the disc plane), we use an exponential decay of the following form:

$$B(z) = B_{\text{disc}} e^{-|z|/z_0}, \quad (3)$$

where  $z_0$  is the scaleheight of the magnetic field, which can be up to four times larger than the scaleheight of the thick synchrotron disc (in the case of equipartition between cosmic rays and magnetic fields, and a synchrotron spectral index  $\simeq 1$ ) (Beck 2001). The thick disc has typically a scaleheight of  $\sim 1.8 \text{ kpc}$ , evidenced from its direct measurement in edge-on galaxies (Dumke & Krause 1998), in agreement with its value for the Milky Way,  $\sim 1.5 \text{ kpc}$  (Beck 2001). Therefore, the magnetic field scaleheight can be as large as 6–7 kpc. Since the LMC is a smaller galaxy (with radius approximately three times smaller than the Milky Way’s), we use in our calculations the value  $z_0 = 2 \text{ kpc}$ .

Let us note that the exponential decay in equation (3) is a conservative choice and can only underestimate the value of the field, since the value of the magnetic field obtained through the RM is already mediated along the line of sight.

**Table 1.** The 23 regions studied. Intensity is measured in mJy beam<sup>-1</sup>.

	RA (J2000)	Dec. (J2000)	Name	$d$ (kpc)	$B_{\text{reg}}$ ( $\mu\text{G}$ )	$B_{\text{tot}}$ ( $\mu\text{G}$ )	$U_{\text{rad}}^{\text{disc}}$ ( $\text{eV cm}^{-3}$ )	$n_{\text{H}}$ ( $\text{cm}^{-3}$ )	$I_{1.4\text{ GHz}}$	$I_{4.8\text{ GHz}}$
1	05:17:43.541	-69:35:17.07	MDM3	0.56	2.45	9.14	1.508	0.07	1.83	1.58
2	05:13:14.664	-69:31:17.19	—	1.21	2.76	10.33	1.346	0.14	1.67	1.27
3	05:17:22.087	-70:20:41.31	MDM1	1.33	1.59	5.96	1.098	0.07	1.56	1.01
4	05:18:51.899	-67:45:54.21	MDM8	1.36	3.61	13.51	1.030	0.07	0.94	0.67
5	05:23:46.213	-68:45:33.88	MDM20	1.51	1.70	6.36	1.207	0.14	2.18	1.47
6	05:10:45.796	-68:05:11.09	—	1.71	2.23	8.34	1.135	0.07	1.40	0.69
7	05:21:50.892	-70:35:46.96	MDM18	1.71	2.45	9.14	0.439	0.07	0.84	0.43
8	05:11:01.258	-69:34:40.98	—	1.72	2.66	9.93	0.857	0.14	1.06	0.60
9	05:22:57.600	-67:29:16.80	MDM17	2.17	5.32	19.86	0.921	0.07	0.80	0.48
10	05:10:21.596	-67:17:12.72	—	2.21	3.08	11.52	0.997	0.54	1.52	0.58
11	05:27:09.571	-67:49:06.69	MDM30	2.73	2.34	8.74	1.266	1.93	2.09	1.69
12	05:28:40.638	-70:35:34.72	MDM32	2.78	2.23	8.34	1.233	0.14	1.50	1.23
13	05:06:19.726	-71:08:26.64	—	3.67	4.04	15.10	0.637	0.07	0.63	0.28*
14	05:26:09.659	-66:00:02.93	—	3.95	4.25	15.89	0.569	0.42	1.63	1.73
15	05:02:44.925	-66:00:28.26	—	4.19	4.57	17.08	0.643	0	0.68	0.36
16	05:34:13.644	-67:55:04.42	MDM58	4.23	2.23	8.34	1.106	0.14	2.11	1.38
17	04:56:57.832	-68:50:35.85	—	4.79	1.70	6.36	0.985	0.24	1.00	0.78
18	05:41:11.743	-68:03:33.24	MDM81	5.77	3.72	13.90	0.601	0.14	0.78	0.38
19	05:40:54.847	-67:41:04.43	MDM82	5.85	3.72	13.90	0.694	0.14	1.12	0.53
20	04:51:36.413	-66:51:26.34	—	6.07	2.34	8.74	0.900	0	0.64	0.28*
21	05:45:23.757	-68:42:57.08	MDM95	6.56	2.76	10.33	0.878	0.14	1.35	0.53
22	05:50:19.691	-69:00:39.60	—	7.64	2.45	9.14	0.494	0.14	1.00	0.62
23	05:51:58.795	-69:45:06.22	MDM113	7.92	2.45	9.14	0.461	0.14	0.46	0.28*

\*Values of intensity lower than the sensitivity (see text).

### 3 DARK MATTER DENSITY PROFILE

The intensity of the radio emission due to WIMP annihilation coming from a given region within the LMC's disc depends on how these particles are distributed in the halo of the LMC. In fact, if  $\rho(r)$  is the density of WIMPs as a function of the galactocentric distance,  $r$ , then the emissivity at a given frequency will be proportional to  $\rho^2(r)$ . We therefore need to estimate  $\rho(r)$  in order to estimate the emission due to DM annihilation.

In Tasitsiomi et al. (2004), different DM density profiles are studied using measurements of the LMC's rotational velocity field. Following this approach, we used the results obtained from H I (Kim et al. 1998) and carbon star data (Alves & Nelson 2000) to estimate  $\rho(r)$ . The H I velocity field is composed of 26 data points at galactocentric distances between  $\sim 0.05$  and  $\sim 3$  kpc. The carbon stars obtained from 422 stars results in four data points, with galactocentric distances between 4.0 and 8.2 kpc. We fit to this data set the following six different DM density profiles suggested in the literature:

(i) A simple isothermal sphere cored profile:

$$\rho_{\text{iso}}(r) = \frac{\rho_0}{1 + (r/r_0)^2};$$

(ii) The Navarro–Frenk–White (NFW) profile, derived from  $N$ -body simulations of CDM haloes for structures ranging from dwarf galaxies to clusters of galaxies (Navarro, Frenk & White 1995, 1996), which diverges as  $\rho \propto r^{-1}$  in the central region of the galaxy:

$$\rho_{\text{NFW}}(r) = \frac{\rho_0}{(r/r_0)[1 + (r/r_0)]^2};$$

(iii) The Moore et al. profile (Moore et al. 1999), derived from independent higher resolution CDM halo simulations, which has a steeper slope than the NFW profile for the central regions of the galaxy ( $\rho \propto r^{-1.5}$ ):

$$\rho_{\text{M}}(r) = \frac{\rho_0}{(r/r_0)^{1.5} [1 + (r/r_0)^{1.5}]};$$

(iv) The Burkert profile (Burkert 1995), that is, a cored profile derived from rotation curve fits of dwarf spiral galaxies:

$$\rho_{\text{B}}(r) = \frac{\rho_0}{[1 + (r/r_0)] [1 + (r/r_0)^2]};$$

(v) The Hayashi et al. profile (Hayashi et al. 2003), which is a modified NFW profile derived from  $N$ -body simulations of the evolution of CDM subhaloes undergoing tidal stripping while orbiting around a larger halo:

$$\begin{aligned} \rho_{\text{H}}(r) &= \frac{f_{\text{t}}}{1 + (r/r_0)^3} \rho_{\text{NFW}}(r) \\ &= \frac{\rho_0}{1 + (r/r_0)^3} \left\{ \frac{1}{(r/r_{0,\text{NFW}})[1 + (r/r_{0,\text{NFW}})]^2} \right\}, \end{aligned}$$

where  $\rho_0 \equiv f \times \rho_{0,\text{NFW}}$ ; and

(vi) The Einasto profile, with three free parameters, first introduced by Einasto (1965) to describe the distribution of stars in our galaxy, and later used to describe the results of  $N$ -body simulations of DM haloes (Navarro et al. 2004):

$$\rho_{\text{E}}(r) = \rho_0 \exp \left\{ -\frac{2}{\alpha} \left[ \left( \frac{r}{r_0} \right)^{\alpha} - 1 \right] \right\}.$$

The NFW, the Moore et al. and the Hayashi et al. profiles were already tested in Tasitsiomi et al. (2004).

The values of the free parameters were determined by fitting each profile to the rotation velocity field using the velocity  $V(r)$  at an orbit of radius  $r$ , inside of which a DM mass  $M(r)$  is enclosed, given by

$$V(r) = \sqrt{\frac{GM(r)}{r}}. \quad (4)$$

The Moore et al. profile gave the worst fit to the data, with a  $\chi^2/\text{d.o.f.} \sim 8$ . The curves that best fitted the other profiles can be seen in Figs 2 and 3 and the resulting values for the free parameters



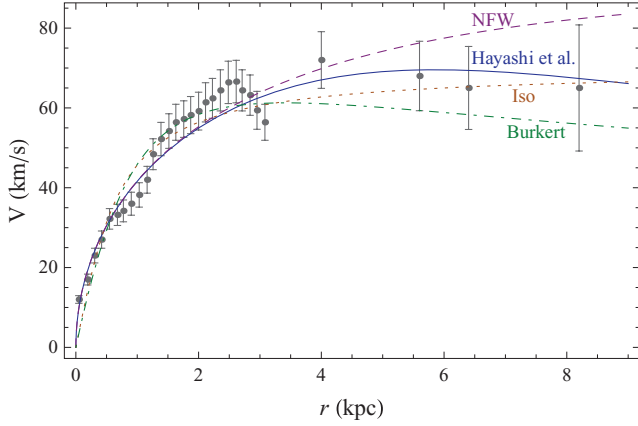


**Figure 2.** Velocity field data points superimposed with the resulting fitted curves for the isothermal sphere, NFW, Burkert and Hayashi et al. density profiles.

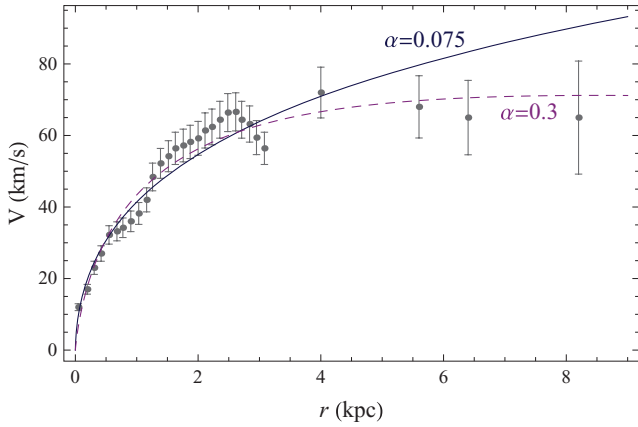


**Figure 3.** Results of fits for the Einasto density profile for  $\alpha = 0.075$ , which resulted in the smallest value of  $\chi^2/\text{d.o.f.}$ , and  $\alpha = 0.3$ .

**Table 2.** Values of the parameters  $\rho_0$  and  $r_0$  and  $\chi^2/\text{d.o.f.}$  obtained from the fit to rotation curve data for each profile.

Profile	$\rho_0$ ( $\times 10^6 \text{ M}_\odot \text{ kpc}^{-3}$ )	$r_0$ (kpc)	$\chi^2/\text{d.o.f.}$
NFW	$8.18 \pm 2.67$	$9.04 \pm 2.43$	1.26
Isothermal sphere	$326 \pm 65$	$0.52 \pm 0.076$	4.23
Burkert	$289 \pm 51$	$1.06 \pm 0.13$	4.54
Hayashi et al.	$8.16 \pm 0.30$	$6.36 \pm 2.08$	1.17
Einasto	$0.0015 \pm 0.0008$	$824 \pm 381$	1.52

for each density profile are displayed in Table 2, as well as the value of the corresponding  $\chi^2/\text{d.o.f.}$  For the purpose of fitting the Hayashi et al. profile, we fixed  $r_{0,\text{NFW}} = 9.04$  kpc, its best-fitting value previously found for the NFW profile.

We can see that both the isothermal sphere and the Burkert profile did not fit well the data, resulting in  $\chi^2/\text{d.o.f.} > 4$ .

For the Einasto profile, we found that good fits (with values of  $\chi^2/\text{d.o.f.}$  around 1.5) can be obtained for values of  $\alpha$  between 0.06 and 0.1. The smallest value of  $\chi^2/\text{d.o.f.}$  was obtained for  $\alpha = 0.075$  and is displayed in Table 2. We can see in Fig. 3 that the resulting curve for  $\alpha = 0.075$  fits very well the rotation curve data for small values of the radius, but does not reproduce its behaviour at larger galactocentric distances. We also plot in Fig. 3 the curve obtained with  $\alpha = 0.3$ . In this case, the fit results in  $\rho_0 = (6.38 \pm$

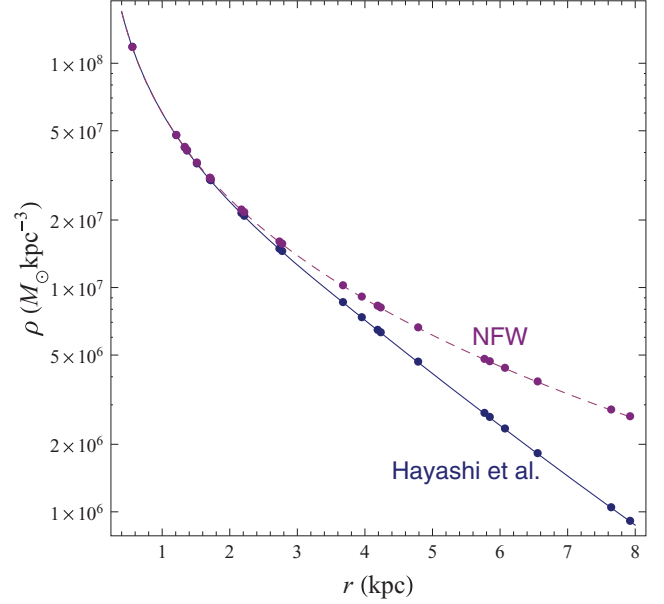


**Figure 4.** NFW and Hayashi et al. density profiles as a function of  $r$  for the best-fitting parameters. The dots show the positions of all the 23 regions.

$1.32) \times 10^6 \text{ M}_\odot \text{ kpc}^{-3}$  and  $r_0 = 4.16 \pm 0.67$  kpc. Although this curve reproduces better the global behaviour of the data, we get a larger value of  $\chi^2/\text{d.o.f.} = 2.05$ . This happens because the small radius points (with smaller error bars) are better fitted by the curve with  $\alpha = 0.075$ .

In any case, the NFW and the Hayashi et al. profiles fit the rotation curve better than the Einasto profile. The behaviour of these two density profiles (with the values of the free parameters set to the ones in Table 2) as a function of the galactocentric distance  $r$  is shown in Fig. 4. We can see that the DM densities predicted by the two profiles are practically the same for  $r \lesssim 2$  kpc. Nevertheless, at the largest distance sampled by our background sources, 7.92 kpc, the difference between the two density profiles is much smaller than one order of magnitude:  $\rho_{\text{NFW}}(7.92 \text{ kpc}) \sim 2.8 \rho_{\text{H}}(7.92 \text{ kpc})$ .

We therefore chose to use the Hayashi et al. density profile in our calculations, both because its fit to the data resulted in the lowest value of  $\chi^2/\text{d.o.f.}$  and because it provides a DM density value lower than the one provided by the NFW profile for most of the regions we are interested in (conservative choice).

## 4 ENERGY-LOSS PROCESSES

While diffusing away from the production site, several energy-loss processes act on the  $e^+e^-$  fluid. Our calculations accounted only for the three fastest energy-loss processes: the synchrotron emission, the ICS off the background photons and bremsstrahlung. We do not include Coulomb energy losses.

### 4.1 Synchrotron

An electron or a positron with energy  $E_e$  diffusing in a region filled with magnetic field  $B$  will lose energy via synchrotron radiation with the following characteristic time-scale:

$$\tau_{\text{syn}} = \tau_{\text{syn}}^0 \left( \frac{B}{\mu\text{G}} \right)^{-2} \left( \frac{E_e}{\text{GeV}} \right)^{-1},$$

where  $\tau_{\text{syn}}^0 = 3.95 \times 10^{17}$  s.

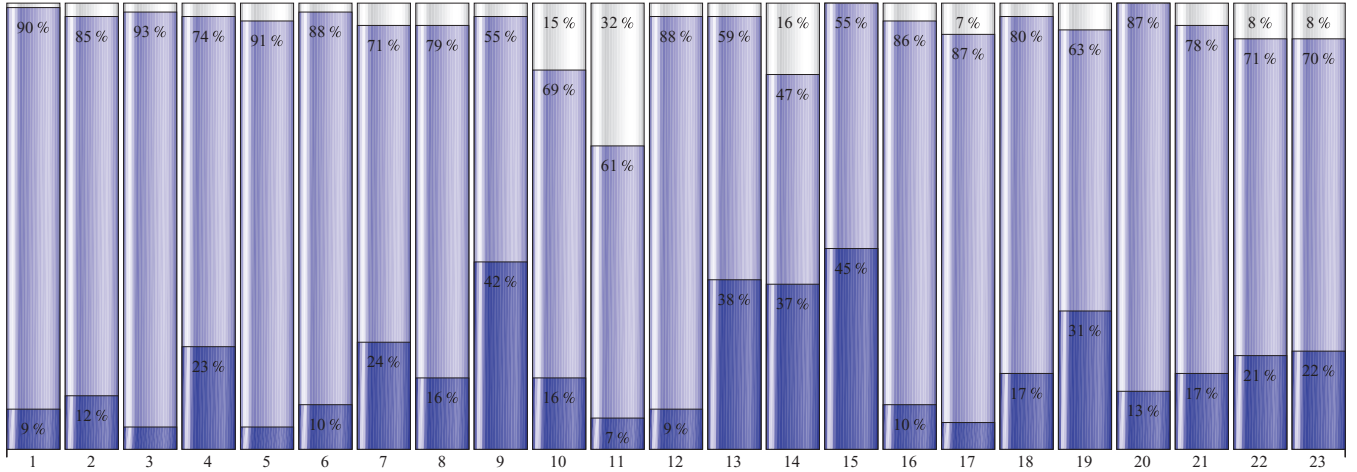


**Figure 5.** Relative contribution of each energy-loss process calculated at the position of each region at 1.4 GHz (see text). The darkest and lightest colours (bottom and upper parts) show the synchrotron and the bremsstrahlung contributions, respectively. The middle parts show the ICS contribution.

## 4.2 Inverse Compton scattering

Similarly, the characteristic time for the ICS is given by

$$\tau_{\text{ICS}} = \tau_{\text{ICS}}^0 \left( \frac{U_{\text{rad}}}{\text{eV cm}^{-3}} \right)^{-1} \left( \frac{E_e}{\text{GeV}} \right)^{-1},$$

where  $\tau_{\text{ICS}}^0 = 9.82 \times 10^{15}$  s and  $U_{\text{rad}}$  is the energy density of the ISRF.

In order to estimate the intensity of the ISRF at the position of each region, we used the map of dust temperature ( $T_d$ ) in the LMC presented in Bernard et al. (2008). The energy density of the ISRF is proportional to  $T_d^{4+\beta}$ . We used  $\beta = 2$  (Boulanger et al. 1996). To obtain the proportionality constant, we used the fact that the dust temperature in the solar neighbourhood is 17.5 K and the local value of the ISRF is  $0.539 \text{ eV cm}^{-3}$  (Weingartner & Draine 2001). We can therefore estimate the ISRF at the position of each one of the 23 regions we are interested in.

Following the same conservative approach we adopted in the case of the magnetic field, we impose that the value of the ISRF obtained in this way corresponds to its value on the disc,  $U_{\text{rad}}^{\text{disc}}$ , and assume that, for each region,  $U_{\text{rad}}$  decays exponentially with  $z$ :

$$U_{\text{rad}}(z) = U_{\text{rad}}^{\text{disc}} e^{-|z|/h_0}, \quad (5)$$

where  $h_0$  is the disc scaleheight, which is actually a function that grows with  $r$  and can be modelled as (Alves & Nelson 2000):

$$h_0(r) = h_0(0) e^{r/\xi} \text{ kpc}, \quad (6)$$

where  $h_0(0) = 0.14$  kpc is the value of the disc scaleheight in the centre of the LMC and  $\xi = 2.24$  kpc.

Table 1 shows the values of  $U_{\text{rad}}^{\text{disc}}$  for all the 23 regions under study.

## 4.3 Bremsstrahlung

The characteristic time for the bremsstrahlung process is given by (Longair 1997):

$$\tau_{\text{brem}} = \tau_{\text{brem}}^0 \left( \frac{n_{\text{H}}}{\text{cm}^{-3}} \right),$$

where  $\tau_{\text{brem}}^0 = 1.17 \times 10^{15}$  s and  $n_{\text{H}}$  is the hydrogen number density.

To estimate the value of  $n_{\text{H}}$  in our selected regions, we used the table of H I clouds in the LMC presented in Kim et al. (2007),

which contains the coordinates, radius and mass of each cloud. We assumed that the clouds are spherical and estimated their density by simply dividing their mass by the volume of a sphere with the reported radius. We then checked if each one of the 23 regions fell inside a cloud and, if so, associated to that region the density of the cloud. If a region fell inside more than one cloud, we associated to that region the density of the highest density cloud, which is a conservative choice. Regions that did not fall inside any cloud were assigned with  $n_{\text{H}} = 0$ . The values of  $n_{\text{H}}$  for each region obtained in this way are reported in Table 1.

We neglect the contribution of ionized hydrogen in our calculations. This is a reasonable approximation in view of the depolarization results obtained in Gaensler et al. (2005), which indicate that there are no bright individual H II regions in the directions where the RMs were observed.

To include the bremsstrahlung in the calculations, we need to modify the  $\mu(\mathbf{r}, \nu)$  function defined in Borriello et al. (2009) to

$$\mu(\mathbf{r}, \nu) = \left\{ \frac{\tau_{\text{syn}}^0}{\tau_{\text{ICS}}^0} \frac{U_{\text{rad}}(\mathbf{r})}{\text{eV cm}^{-3}} + \frac{\tau_{\text{syn}}^0}{\tau_{\text{brem}}^0} \sqrt{\frac{\nu_0 B(\mathbf{r})}{\nu}} \frac{n_{\text{H}}}{\mu\text{G cm}^{-3}} + \left[ \frac{B(\mathbf{r})}{\mu\text{G}} \right]^2 \right\}^{-1},$$

where  $\nu$  is the frequency and  $\nu_0 = 3.7 \times 10^6$  Hz.

Fig. 5 compares the energy-loss rate,  $b = E_e/\tau$ , for each of the three energy-loss processes, at the position of all the 23 regions. For each region, we plot the values of the normalized energy-loss rate for the synchrotron (calculated using  $B_{\text{reg}}$ ), ICS and the bremsstrahlung processes. All the values were evaluated on the plane of the disc ( $z = 0$ ) and we used the frequency peak approximation  $E_e = \sqrt{B_{\text{reg}} \times \nu/\nu_0}$  GeV, where  $B_{\text{reg}}$  is measured in  $\mu\text{G}$ . Since the results were very similar for  $\nu = 1.4$  and 4.8 GHz, we show only the results obtained for 1.4 GHz.

While ICS is clearly the dominant process in all regions we are studying, the contribution of bremsstrahlung seems to be the smallest one. It is, however, surely not negligible in at least three regions (10, 11 and 14). These processes therefore cannot be neglected.

If we remember that the regions are numbered according to their galactocentric distance, we immediately notice in Fig. 5 the apparent lack of correlation between the energy-loss rates (and therefore of

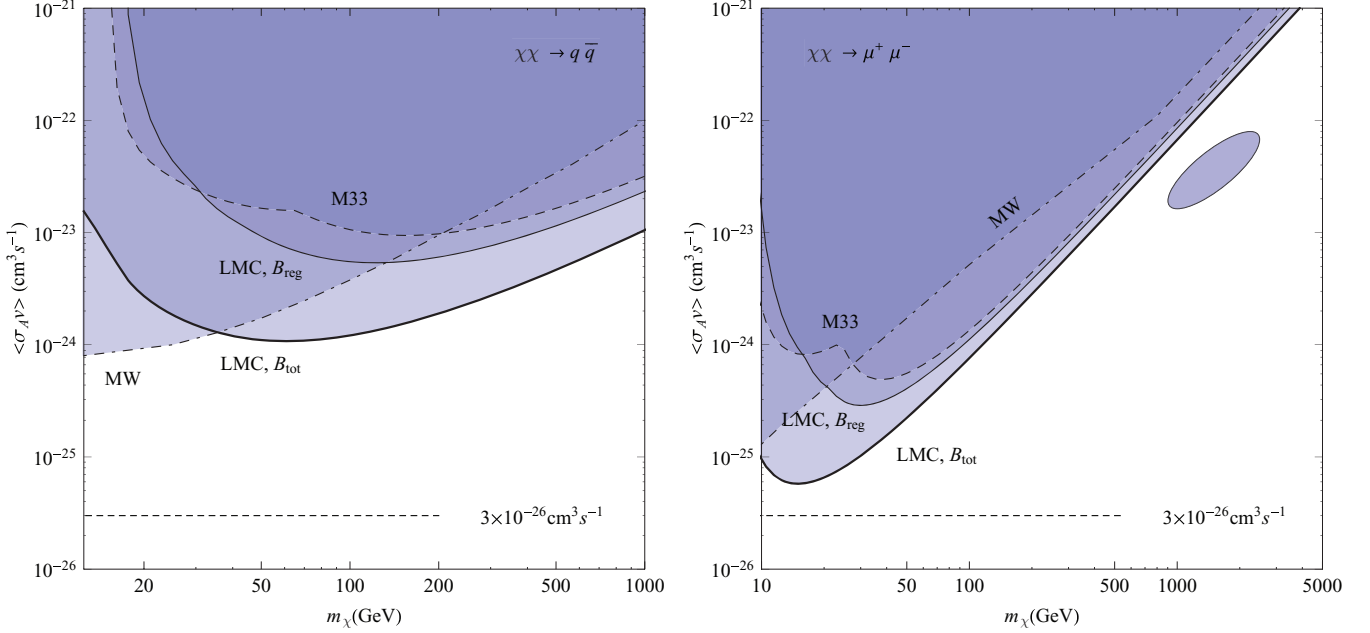


**Figure 6.** Constraints obtained with the  $\chi\chi \rightarrow b\bar{b}$  channel (left-hand panel) and the  $\chi\chi \rightarrow \mu^+\mu^-$  channel (right-hand panel). The solid lines indicate the best constraints obtained with the LMC using either  $B_{\text{tot}}$  or  $B_{\text{reg}}$ . The dashed lines indicate the best constraints obtained with M33 (Borriello et al. 2010) and the dot-dashed lines indicate those obtained with the Milky Way (Borriello et al. 2009). The shaded regions are the forbidden ones. The ellipse shaped region indicates the region favoured by the PAMELA/HESS/Fermi-LAT results (Meade et al. 2010).

the magnetic field, the ISRF and the hydrogen distribution) and the galactocentric distance, which is clearly a consequence of the irregular nature of the LMC.

## 5 RESULTS

We considered two possible WIMP annihilation channels:  $\chi\chi \rightarrow b\bar{b}$ , in which electrons and positrons will be produced by decaying muons ( $\mu^- \rightarrow e^- \bar{\nu}_e \nu_\mu$ ) and anti-muons ( $\mu^+ \rightarrow e^+ \bar{\nu}_\mu \nu_e$ ) produced in pion decays ( $\pi^- \rightarrow \mu^- \bar{\nu}_\mu$  and  $\pi^+ \rightarrow \mu^+ \nu_\mu$ ) and the leptophilic channel  $\chi\chi \rightarrow \mu^+\mu^-$ .

Leptophilic channels have recently raised interest in view of the experimental results on the electron/positron cosmic-ray spectra. While PAMELA observed an unexpected rise in the positron fraction (Adriani et al. 2009), Fermi-LAT observes a deviation from a simple power-law spectrum (Abdo et al. 2009), thus confirming the previous results obtained by the HESS (Aharonian et al. 2009). If these results are to be interpreted as due to DM annihilation in the galactic halo, one needs to consider leptophilic channels and high mass scales (see the recent discussions by Bergstrom, Edsjo & Zaharijas 2009; Meade et al. 2010).

The synchrotron intensity at a frequency  $\nu$  due to DM annihilation coming from a region inside a solid angle  $d\Omega$  on the LMC's disc is

$$\frac{dI}{d\Omega} = \frac{\cos i}{4\pi} \int j_\nu(\mathbf{r}, z) ds, \quad (7)$$

where  $i$  is the disc inclination,  $s$  is the distance along the line of sight and  $j_\nu(\mathbf{r}, z)$  is the synchrotron emissivity at a position in the LMC's halo with galactocentric distance  $\mathbf{r}$  along the disc and height  $z$  above or below the disc. The term  $\cos i$  accounts for the fact that the line of sight is not parallel to  $z$ .

The expression of the emissivity is derived in detail in Borriello et al. (2009).

We evaluated equation (7) for all 23 regions using  $\nu = 1.4$  and 4.8 GHz. The most constraining results were obtained for 1.4 GHz and can be seen in Fig. 6 for both annihilation channels considered. For comparison, we show also the best constraint obtained in Borriello et al. (2010) for M33 using an NFW profile and assuming equipartition between magnetic fields and cosmic rays, and the best constraint obtained in Borriello et al. (2009) for the Milky Way using the  $\chi\chi \rightarrow b\bar{b}$  channel. For the  $\chi\chi \rightarrow \mu^+\mu^-$  channel, we show the best constraint obtained for the Milky Way using the same formalism and observations described in Borriello et al. (2009) and also the favoured region obtained when one attributes to DM annihilation the experimental results described above (Meade et al. 2010).

## 6 SUMMARY AND DISCUSSION

We have imposed constraints on the  $m_\chi - \langle\sigma_A v\rangle$  plane using radio observations at 1.4 and 4.8 GHz of the LMC and analysing two different DM annihilation channels, a hadronic and a leptonic one.

The existence of high-resolution observations of the LMC in several frequency bands has allowed us to obtain most of the information needed to calculate the DM annihilation signal, making the least possible number of hypotheses in all the steps of the calculation. Being able to escape from this problem and, when necessary, making conservative assumptions, we have therefore obtained very robust results.

In all cases studied, the best constraints were obtained using 1.4 GHz, since the number of  $e^-$  and  $e^+$  produced by DM annihilation decreases with energy. For higher frequencies to produce competing constraints, the observed intensity at those frequencies should be much lower than at 1.4 GHz.

From Fig. 6, we can see that the constraints on the  $m_\chi - \langle\sigma_A v\rangle$  plane imposed from the analysis of the LMC are stronger than the

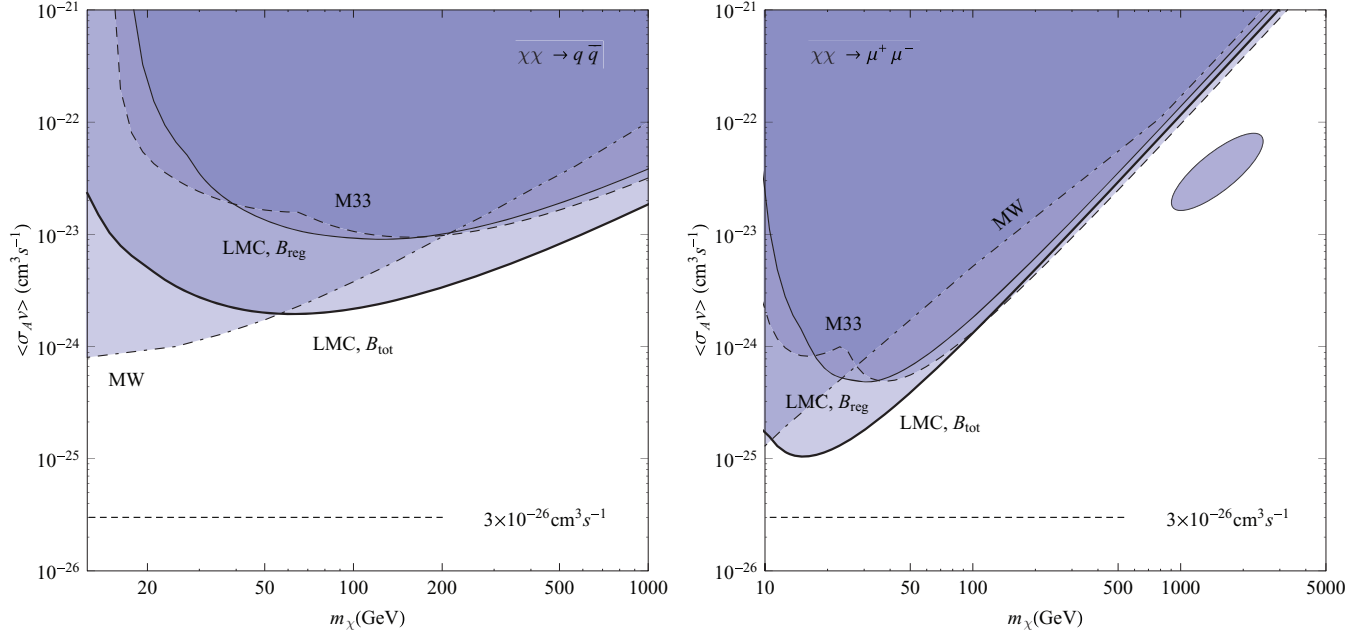


**Figure 7.** Same as Fig. 6, but using the isothermal sphere DM density profile with the parameters obtained in Alves & Nelson (2000).

ones obtained with M33 and with the Milky Way over most of the mass range considered, excluding very low mass regions.

In Tasitsiomi et al. (2004), the estimated DM annihilation signal at various frequencies was obtained, fixing  $m_\chi = 50$  GeV and  $\langle \sigma_A v \rangle = 2 \times 10^{-26} \text{ cm}^3 \text{s}^{-1}$  and using a constant magnetic field of intensity of either  $B = 5$  or  $18.4 \mu\text{G}$ . We can estimate from their fig. 5 that at 1.4 GHz they obtain  $\langle \sigma_A v \rangle \lesssim 4 \times 10^{-25} \text{ cm}^3 \text{s}^{-1}$  for  $B = 5 \mu\text{G}$  and  $\langle \sigma_A v \rangle \lesssim 3 \times 10^{-25} \text{ cm}^3 \text{s}^{-1}$  for  $B = 18.4 \mu\text{G}$ . From Fig. 6, we can see that for  $m_\chi = 50$  GeV our best constraints using the hadronic channel are  $\langle \sigma_A v \rangle < 9.25 \times 10^{-24} \text{ cm}^3 \text{s}^{-1}$  using only  $B_{\text{reg}}$  and  $\langle \sigma_A v \rangle < 1.10 \times 10^{-24} \text{ cm}^3 \text{s}^{-1}$  using  $B_{\text{tot}}$ . This result can be explained by the hypotheses adopted in Tasitsiomi et al. (2004), which have overestimated the DM annihilation signal. In the first place, inspection of Table 1 shows that imposing a constant magnetic field of  $18.4 \mu\text{G}$  for the entire volume of the LMC is not realistic. Even if we take into account only the  $B_{\text{tot}}$  column, we see that more than half of the regions present  $B_{\text{tot}} < 10 \mu\text{G}$ . As for the hypothesis  $B = 5 \mu\text{G}$ , we can see from Fig. 5 that the bremsstrahlung and, in particular, the ICS processes cannot be neglected (see e.g. regions 9 and 15, for which  $B_{\text{reg}} = 5.32$  and  $4.57 \mu\text{G}$ , respectively). In fact, if we do neglect these two processes in our calculations, our results improve by a factor of  $\sim 3$ .

Finally, we would like to comment on one possible shortcoming of our analysis. When fitting the LMC's rotation curve, we took into consideration only the DM mass, ignoring the luminous matter. To understand the effect of this choice, we again carried out our calculations using the results obtained in Alves & Nelson (2000), where an isothermal sphere density profile is fitted to the LMC's rotation curve after subtracting the disc component (stars + gas). The resulting values of the free parameters are  $\rho_{\text{iso}} = 10^8 \text{ M}_\odot \text{kpc}^{-3}$  and  $r_{\text{iso}} = 1 \text{ kpc}$ . Using this density profile, the best constraints were obtained at 1.4 GHz and can be seen in Figs 7(a) and (b).

We can see that, accounting for the luminous matter in this way, our results are not very much affected and the conclusions previously described are still valid.

## ACKNOWLEDGMENTS

We would like to thank Maurizio Paolillo for fruitful discussions and Jean-Philippe Bernard for kindly sending us the dust temperature data. GM would like to thank the partial support of MIUR - PRIN2008 'Fisica Teorica Astroparticellare'.

## REFERENCES

- Abdo A. A. et al., 2009, Phys. Rev. Lett., 102, 181101
- Abdo A. A. et al., 2010, ApJ, 712, 147
- Adriani O. et al., 2009, Nat, 458, 607
- Aharonian F. et al., 2009, A&A, 508, 561
- Aloisio R., Blasi P., Olinto A. V., 2004, JCAP, 05, 007
- Alves D. R., 2004, New Astron. Rev., 48, 659
- Alves D. R., Nelson C. A., 2000, ApJ, 542, 789
- Baltz E. A., Wai L., 2004, Phys. Rev. D, 70, 023512
- Barger V., Halzen F., Hooper D., Kao C., 2002, Phys. Rev. D, 65, 075022
- Beck R., 2001, Space Sci. Rev., 99, 243
- Bergstrom L., Edsjo J., Zaharijas G., 2009, Phys. Rev. Lett., 103, 031103
- Bergstrom L., Fairbairn M., Pieri L., 2006, Phys. Rev. D, 74, 123515
- Bernard J.-P. et al., 2008, AJ, 136, 919
- Blasi P., Olinto A. V., Tyler C., 2003, Astropart. Phys., 18, 649
- Borriello E., Cuoco A., Miele G., 2009, Phys. Rev. D, 79, 023518
- Borriello E., Longo G., Miele G., Paolillo M., Siffert B. B., Tabatabaei F. S., Beck R., 2010, ApJ, 709, L32
- Boulanger F., Abergel A., Bernard J.-P., Burton W. B., Desert F.-X., Hartmann D., Lagache G., Puget J.-L., 1996, A&A, 312, 256
- Burkert A., 1995, ApJ, 447, L25
- Colafrancesco S., Profumo S., Ullio P., 2006, A&A, 455, 21
- Colafrancesco S., Profumo S., Ullio P., 2007, Phys. Rev. D, 75, 023513
- Crawford F., Kaspi V. M., Manchester R. N., Lyne A. G., Camilo F., D'Amico N., 2001, ApJ, 553, 367
- Crocker R. M., Bell N. F., Balázs C., Jones D. I., 2010, Phys. Rev. D, 81, 063516
- Dickel J. R., McIntyre V. J., Gruendl R. A., Milne D. K., 2005, AJ, 129, 790

- Dumke M., Krause M., 1998, in Breitschwerdt D., Freyberg M. J., Truemper J., eds, *Proc. IAU Symp. 166, Lecture Notes in Phys. Vol. 506, The Local Bubble and Beyond*. Springer-Verlag, Berlin, p. 555
- Einasto J., 1965, *Trudy Inst. Astrofiz. Alma-Ata*, 51, 87
- Feng J. L., 2010, preprint (arXiv:1003.0904)
- Gaensler B. M., Haverkorn M., Staveley-Smith L., Dickey J. M., McClure-Griffiths N. M., Dickel J. R., Wolleben M., 2005, *Sci*, 307, 1610
- Gondolo P., 1994, *Nuclear Phys. B Proc. Suppl.*, 35, 148
- Hayashi E., Navarro J. F., Taylor J. E., Stadel J., Quinn T., 2003, *ApJ*, 584, 541
- Hooper D., 2008, *Phys. Rev. D*, 77, 123523
- Hughes A., Staveley-Smith L., Kim S., Wolleben M., Filipović M., 2007, *MNRAS*, 382, 543
- Kim S., Staveley-Smith L., Dopita M. A., Freeman K. C., Sault R. J., Kesteven M. J., McConnell D., 1998, *ApJ*, 503, 674
- Kim S. et al., 2007, *ApJS*, 171, 419
- Longair M., 1997, *High Energy Astrophysics Vol. 1: Particles, Photons and their Detection*. Cambridge Univ. Press, Cambridge
- Marx M., Dickey J. M., Mebold U., 1997, *A&AS*, 126, 325
- Meade P., Papucci M., Strumia A., Volansky T., 2010, *Nuclear Phys. B*, 831, 178
- Moore B., Quinn T., Governato F., Stadel J., Lake G., 1999, *MNRAS*, 310, 1147
- Navarro J. F., Frenk C. S., White S. D. M., 1995, *MNRAS*, 275, 720
- Navarro J. F., Frenk C. S., White S. D. M., 1996, *ApJ*, 462, 563
- Navarro J. F. et al., 2004, *MNRAS*, 349, 1039
- Tasitsiomi A., Gaskins J., Olinto A. V., 2004, *Astropart. Phys.*, 21, 637
- van der Marel R. P., Cioni M.-R. L., 2001, *AJ*, 122, 1807
- van der Marel R. P., Kallivayalil N., Besla G., 2009, *Proc. IAU Symp. 256, The Magellanic System: Stars, Gas, and Galaxies*. Cambridge Univ. Press, Cambridge, p. 81
- Weingartner J. C., Draine B. T., 2001, *ApJS*, 134, 263
- Zhang L., Sigl G., 2008, *JCAP*, 09, 027

This paper has been typeset from a  $\text{\LaTeX}$  file prepared by the author.